Probabilistic Engineering Mechanics 37 (2014) 41–50

Contents lists available at ScienceDirect

Probabilistic Engineering Mechanics

journal homepage: www.elsevier.com/locate/probengmech

Analysis of the probability of failure for open-grown trees during wind storms

Cihan Ciftci [a,b,*], Sanjay R. Arwade [b], Brian Kane [c], Sergio F. Brena [b]

[a] Department of Civil Engineering, Abdullah Gul University, Turkey
[b] Department of Civil and Environmental Engineering, University of Massachusetts, Amherst, MA, USA
[c] Department of Environmental Conservation, University of Massachusetts, Amherst, MA, USA

ARTICLE INFO

Article history:
Received 26 November 2013
Received in revised form
5 April 2014
Accepted 7 April 2014
Available online 18 April 2014

Keywords:
Trees
Wind
Storms
Probabilistic analysis

ABSTRACT

Although trees convey important environmental, economic, and sociological benefits on humans and society, they can also cause significant economic and societal disruptions, especially when subjected to wind storms in urban environments. Tools for proper assessment of the risk of these disruptions can be of significant benefit to society. In this research an approach to quantifying the failure probability for trees subject to wind storms is presented and illustrated by application to two specific maple trees in Massachusetts, USA. The approach entails four specific steps: (1) Random wind time history samples were generated using a modified Ochi–Shin spectrum, (2) these wind time histories were used as loading time histories on finite element models of the example trees in both summer (in-leaf) and winter (leafless), (3) maximum bending moments generated by the random wind time histories were compared to the failure (yield) moment of the tree at 1.4 m above ground, (4) the failure/fragility curves of the trees were estimated by Monte Carlo simulation for a range of average wind speeds and for 1000 independent wind time histories at each wind speed.

1. Introduction

Trees growing in residential settings (amenity trees) provide many environmental, economic, and sociological benefits [1], but tree failure can damage property and injure people—sometimes fatally [2]. Property damage and personal injury sometimes lead to costly litigation [3]. Arborists attempt to mitigate tree failure by proactively assessing risk [4], which is a combination of the probability of failure and the consequences of that failure. Wind is the primary cause of tree failure in many climates [5,6], and has been a subject of investigation in forestry for many years. Three different approaches have been developed: (1) qualitative assessments, (2) empirical or statistical models, (3) mechanistic models [7]. The first approach is based on observational tools [8,9]. The second approach provides better accuracy for a range of locations [3]. The third approach, using mechanistic models, is the most recent approach although it has been pointed out that mechanistic models, due to their deterministic nature and limitations in the idealization complicated systems such as trees, sometimes provide predictions which conflict with field observations [7]. Since the initial efforts to develop GALES [5] and HWIND [10], others (such as [11]) have continued model development. The FOREOLE model [12] considers both wind and snow loading in estimating the probability of failure. All of the models consider forest- or plantation-grown trees, which are morphologically different from amenity trees. The latter typically have broader crowns, more and larger branches, and a more tapered stem that often splits into multiple, co-dominant stems.

In addition to considering amenity trees rather than forest or plantation trees, another novel aspect of the current study is the consideration of the failure of individual trees, whereas most previous models operate on the scale of the forest stand or plantation. The current study also employs finite element (FE) modeling while considering randomness in wind speeds, evaluating tree response based on a dynamic time history analysis. Existing mechanistic models attempt to capture the complex tree dynamics with an empirically-determined gust factor [7], that may have limited application outside of the region where it was determined. The use of Monte Carlo (MC) simulations, while computationally expensive [13], is a conventional method in probabilistic structural analysis. For systems with appreciable probabilities of failure, such as trees, MC simulations can provide accurate results with a relative degree of efficiency. The analysis of probability of failure that is at the heart of this method computes the cumulative probability of system failure at specified mean

* Corresponding author at: Department of Civil Engineering, Abdullah Gul University, Turkey. Tel.: +90 553 379 0785.
E-mail address: cihanc58@gmail.com (C. Ciftci).

http://dx.doi.org/10.1016/j.probengmech.2014.04.002
0266-8920/

wind speeds [14]. In the current case, failure is defined as occurring when the bending moment at 1.4 m induced by the wind exceeds the bending moment capacity of the stem at 1.4 m. The moment capacity is defined as the moment that generates extreme fiber compressive stress equal to the compressive yield stress of the wood.

The objective of this study is to propose a method for estimating the probability of failure at specified mean wind speeds leading to failure/fragility curves for amenity trees due to wind storms. The method described here is broadly applicable to probabilistic analysis of trees using many possible sets of modeling assumptions. To show how the method may be applied in practice and to provide guidance in presenting and interpreting results, failure/fragility curves are presented for two example sugar maple trees (*Acer saccharum* Marsh.). Additionally, this study includes the effect of decay and leaves on the probability of failure. The examples are instructive regarding application of the method and interpretation of results, but within the scope of this paper several key modeling assumptions regarding tree geometry, aerodynamic characteristics and dynamics have been made. In applying the proposed method to trees for the purpose of a complete risk analysis these assumptions should be carefully considered and in some cases more detailed or complicated models may be appropriate.

2. Methods

2.1. Modeling approach and parameters

Dynamic time history analysis of a 3D finite element model of the trees is at the core of the proposed approach. This approach has previously been used by the authors in a deterministic study of tree dynamics [15]. The finite element models use beam elements of varying cross sectional dimensions to model stem and branch taper, assume a fixed support condition at the base, 5% damping for the winter state of the tree and 15% damping for the summer state of the tree (the large difference in damping is due to the additional aerodynamic damping provided by the leaves). The summer damping of Tree-1 was measured at 15% [16]. Winter damping of 5% was assumed based on [17,18] who found that summer damping was three times winter damping for Bradford pears (*Pyrus calleryana* Decne. 'Bradford') and red oaks (*Quercus rubra* L.). Because the crown width of Tree-9 was similar to Tree-1 and Kane et al. [16] found that crown width of sugar maples was proportional to damping, Tree-9 was assumed to have the same summer and winter damping ratios. This assumption was made in the absence of an experimental measurement and consistent with the literature cited above. Experimental measurement of the four damping cases (Trees 1 and 9 in summer and winter) would certainly improve the accuracy of the finite element models. However, to illustrate the application of the method described here, simplifying assumptions regarding damping have been made that, in light of the existing literature and some recent measurements, are reasonable. The two sugar maple trees are located (1) in Belchertown, MA (42.28018°N, 72.407735°W) and (2) at the University of Massachusetts, Amherst, MA (42.273278°N, 72.414547°W) and were modeled using ADINA 8.5 (ADINA Software, Watertown, MA, USA). Photographs and FE models of both trees are shown in Fig. 1. The size and crown architecture of each tree were measured as described in [15]. Tree-1 has 10 branches and a stem diameter of 0.53 m, while Tree-9 has 29 branches and a stem diameter of 0.66 m. Material properties were assumed from [19,20] as described in [15]. Drag (F_D) on each segment in the FE model was calculated as

$$F_D = \tfrac{1}{2}\rho U^2 A C_D \tag{1}$$

where ρ is the air density [kg/m^3], A is frontal area [m^2], U is wind speed [m/s], and C_D is the non-dimensional drag coefficient. It is important to note that Eq. (1) neglects the interaction between the dynamically deforming tree and the wind field—a variety of fluid structure interaction. Such interactions can be meaningful [21,22] but modeling such interactions in dynamic time history analysis within a Monte Carlo framework is computationally prohibitive within the scope of this study since modeling such interactions requires a computational fluid dynamics model capable of modeling turbulence at length scales smaller than branch diameter as well as a structural mechanics model. Coupling the models imposes additional, significant, computational burdens. The first order calculation of wind loading presented in Eq. (1) has therefore been adopted here. Since wind speed varies with height (z) above ground [23,24], U was assumed to vary with height (z) according to the relationship proposed by [25]

$$U(z) = U_h\left(\frac{z}{h}\right)^{1/7} \tag{2}$$

where U_h is the reference wind speed at height h.

The response of each tree was modeled in winter and summer. In temperate climates, several relevant parameters change between the seasons. In addition to different values of ρ (1.226 kg/m^3 for summer and 1.326 kg/m^3 for winter), C_D was assumed to be 1 in winter (because stem and branch segments were modeled as cylinders). In summer, C_D was assumed to vary with U in accordance with an empirical relationship [26]. Frontal area in winter was defined as the exposure area of the stem and the branches (modeled as cylinders); in the summer, it was estimated from an empirical relationship for smaller red maples (*Acer rubrum* L.) (Kane, unpublished data, see Fig. 2). For Tree-1 and Tree-9, frontal area in summer was 3.9 and 2.5 times, respectively, larger than frontal area in winter. Estimation of frontal area from tree morphometry was necessary in this case because photographs of the trees did not allow direct measurement of the frontal area due to the presence of significant background vegetation. Published studies on the relationship of leaf area to stem diameter [27–29] show that such predictions are generally possible, but none of those studies address frontal area rather than leaf surface area and none include trees from the northeast United States. The data of Fig. 2 have therefore been used to predict frontal area. The data were collected using an established method [26] that has been used to assess frontal area of multiple tree species [30]. The data reflect smaller trees of a different species than the trees studied here, but Nowak [27] has shown that relationships between morphometry and leaf area are largely consistent across species and genera. Although there are many intricacies in predicting the frontal area of these trees, consistently using an established method to predict frontal area makes it reasonable to apply the probabilistic approach described here since the primary objective is to introduce the method and compare two trees for which it was not possible to measure frontal area accurately.

2.2. Stochastic wind model

The Ochi–Shin equation

$$S_{Vw}(\omega) = \frac{C V_w^2 F_g}{\omega} \tag{3}$$

which had been developed to define the wind spectrum for offshore areas [31], was modified to correspond to the local terrain of the example trees by altering the surface drag coefficient (C).

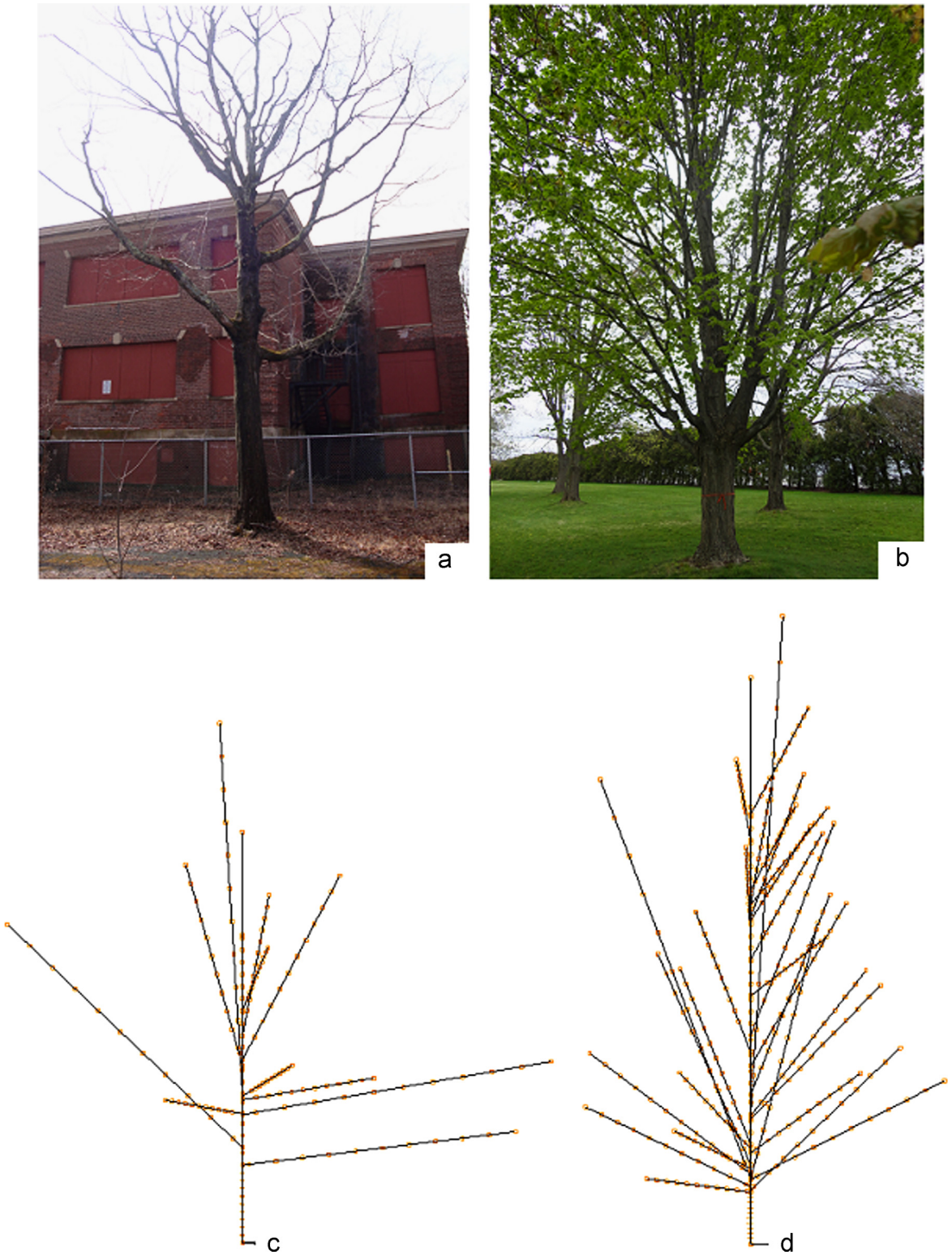

Fig. 1. Photos and models of the trees. The left figures (a, and c) are for Tree-1 in Belchertown, MA, and the right figures (b, and d) are for Tree-9 on the campus of the University of Massachusetts in Amherst, MA.

The Ochi–Shin spectrum was selected, rather than a spectrum developed specifically for agricultural meteorology problems [32–38] because it was able to fit the measured data through modification of a single, physically meaningful parameter, the surface drag coefficient C. The agricultural models, on the other hand, contain canopy and tree-specific parameters that, while they could have been fit to the data collected here, would have provided a less physically meaningful fit. In applying the method presented here, an alternative appropriate spectrum could be substituted without changing the method. This coefficient was increased due to the larger surface roughness found over land than offshore. In Eq. (3), $S_{Vw}(\omega)$ is the wind speed spectral density; C is the surface drag coefficient, which is related to surface roughness; V_w is the average wind speed (m/s) at a reference height of 10 m; ω is the

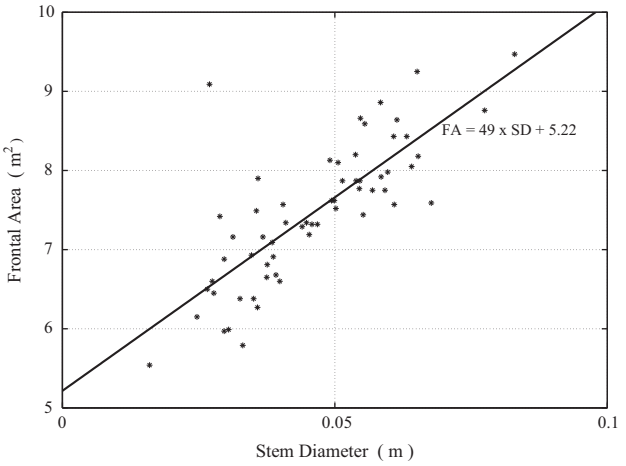

Fig. 2. The relationship between stem diameter and frontal area with leaves. The equation of the linear fit to the experimental data is Frontal Area=49 × (Stem Diameter)+5.22.

wind frequency (rad/s); and F_g is the gust factor

$$F_g = \begin{cases} 583((1.592\omega)/V_W) & 0 \le \omega \le 0.001885V_W \\ \frac{420((1.592\omega)/V_W)^{0.7}}{(1+((1.592\omega)/V_W)^{0.35})^{11.5}} & 0.001885V_W \le \omega \le 0.0628V_W \\ \frac{838((1.592\omega)/V_W)}{(1+((1.592\omega)/V_W)^{0.35})^{11.5}} & 0.0628V_W \le \omega \end{cases} \quad (4)$$

The specific modification made involved the calculation of the spectral densities of time histories of wind-speed measured in Amherst, MA. These spectra were then compared with Eq. (3), and C, originally defined as

$$C = (750+69V_w)(1.0 \times 10^{-6}) \quad (5)$$

was modified to

$$C^M = (20000+69V_w)(3.7 \times 10^{-6}) \quad (6)$$

The spectral densities of the field data can be seen in Fig. 3 with the modified Eq. ((6) placed into (3)). The modified surface drag coefficient, C^M in Eq. (6), is specific to land areas of Amherst, MA. If analysis for another site is desired a suitable site specific wind spectrum would be required.

In the FE model, drag force was developed for 13 m/s $\le V_w \le$ 39 m/s in increments of 2 m/s for a reference height (1.4 m above ground). In order to calculate this drag force for each element of the tree models, four steps were followed. First, for each increment of V_W (wind-speed), 1000 samples were randomly generated by substituting Eqs. (4) and (6) into Eq. (3) and using the spectral representation method [39] given by

$$V_w^G(t) = \sum_{r=1}^{n} A_r \sin(\omega_r t) + B_r \cos(\omega_r t) \quad (7)$$

where A_r and B_r are independent Gaussian random variables with zero mean and variance

$$\sigma_r^2 = G_{VV}(\omega_r)\Delta\omega \quad (8)$$

where $G_{VV}(\omega_r)$ is the value of the one-sided spectral density at ω_r and $\Delta\omega$ is the interval of frequencies for equally divided frequency range. The spectral density was divided into 430 equal parts (n=430) from 0.00 to approximately 0.48 Hz in order to obtain a time-history of the stochastic process that did not exhibit periodicity over a period of approximately 15 min.

Second, the Nataf model [40]

$$V_i = \frac{\mu_{X_i}^2}{\sqrt{\mu_{X_i}^2+\sigma_{X_i}^2}} \exp\left(V_i^G \sqrt{ln\left(\frac{\mu_{X_i}^2+\sigma_{X_i}^2}{\mu_{X_i}^2}\right)}\right) \quad (9)$$

in which V_i^G is a Gaussian variable and μ_{X_i} and $\sigma_{X_i}^2$ are the mean and variance, respectively, of the targeted log-normally distributed wind speed random variables (V_i), was applied to convert the Gaussian samples into time histories with lognormal marginal distribution, which is a commonly used distribution type for wind-speed records [41–43]. Although the Nataf transformation distorts the spectrum in the non-Gaussian space from that in the Gaussian space, this distortion was found to be small (< 1%) and has been neglected. An example time history of one of these samples is shown in Fig. 4.

Third, the resulting non-Gaussian wind-speed samples were adjusted for the heights of each element of the tree models by using Eq. (2).

Fourth, Eq. (1) was applied to calculate the drag forces for each element of the FE tree models.

2.3. Probability of failure estimation

Failure of a tree during a time interval was defined as occurring when the maximum wind-induced bending stress due to moment exceeded the compressive yield stress in the stem at 1.4 m above ground. This is equivalent to the maximum bending moment exceeding the yield moment. Using this definition, the probability of failure is equivalent to the probability of exceedance as usually defined in the theory of stochastic processes. Therefore, the probability of failure (P_f) in a given time period (T) can be calculated:

$$P_f(\xi, T) = \text{Prob}\left[\max_{t\epsilon[0,T]} M(t) \ge \xi\right] \quad (10)$$

where ξ is the threshold, that is, the yield moment, and $M(t)$ is the random time history of generated moments from the FE model. An example of the moments generated during a 15-min interval in the FE model is shown in Fig. 5. The threshold value of the bending moment ($M_y = \xi$) in Fig. 5 can be calculated as

$$M_y = \frac{\pi\sigma_y D^3}{32} \quad (11)$$

which is simply the flexure formula for a solid circular cross section solved for M_y. The yield stress (σ_y) is the compression strength parallel to grain (27.7 MPa from [20]) and D is the diameter of the stem at 1.4 m above ground. Fifteen minute time histories were chosen as representative of extreme condition durations during typical wind storms.

In the research of Ciftci et al. [44], the effect of decay in tree cross-section on the moment capacity loss (MCL) of the cross-section was investigated. Using this approach, MCL can be estimated for any decay location and decay size in the cross-section. This provides a straightforward way of evaluating the effect of decay on failure probability that does not require the recalculation of the entire dynamic time history, provided that it can be assumed that the decay is localized enough to not substantially change the overall tree dynamics and therefore the moment demand. This assumption has been assessed for the trees studied here and when moment capacity loss is equal to or less than 20% and the vertical extent of the decay is 50 cm the effect of decay on tree dynamics is indeed negligible (< 1% difference in dynamic amplification). If a tree with much larger vertical extent of decay and a much larger percentage of moment capacity loss were to be studied, it would be appropriate to reassess the validity of this assumption. Results that follow will include consideration of the effect of MCL on probability of failure.

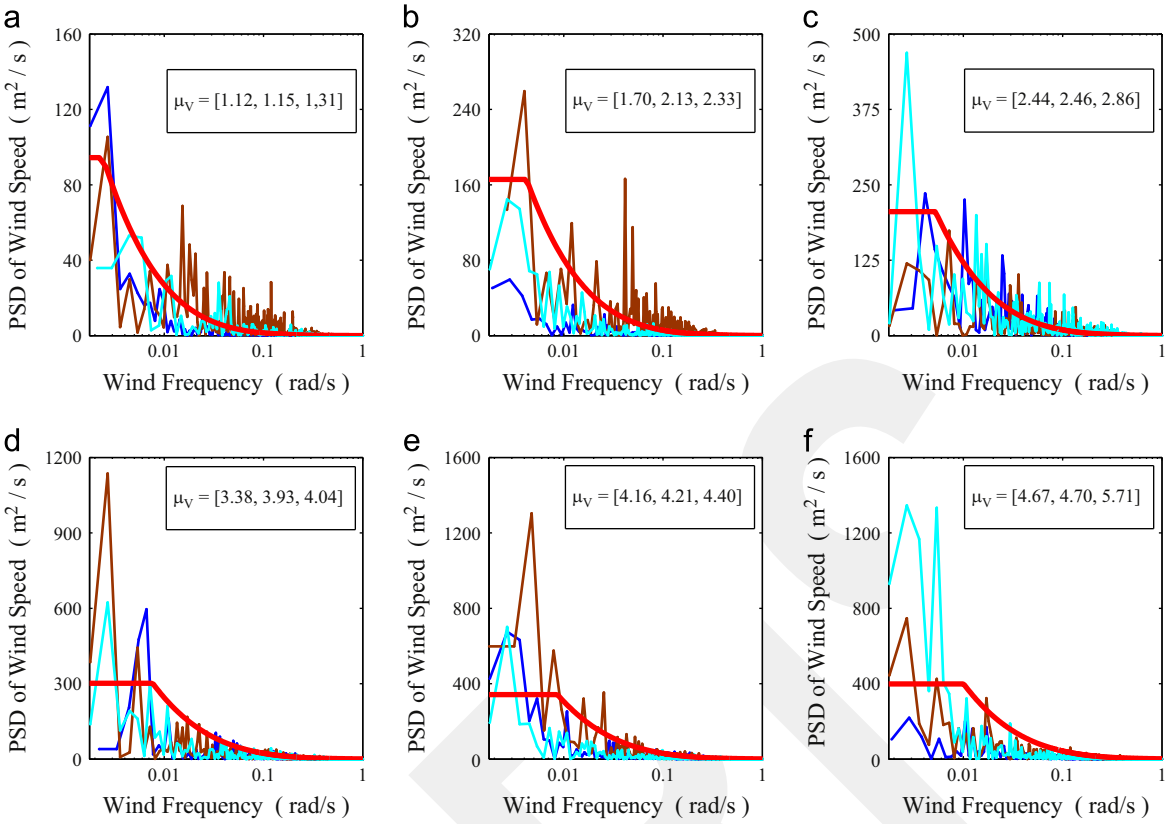

Fig. 3. Comparison of wind spectral densities of field data and modified Ochi–Shin equation. Each frame shows experimentally derived spectra from observations of wind records for a narrow range of mean wind speeds and the corresponding adjusted Ochi–Shin spectrum. (a) Modified Ochi–Shin for 1.19 m/s, (b) Modified Ochi–Shin for 2.05 m/s, (c) Modified Ochi-Shin for 2.59 m/s, (d) Modified Ochi-Shin for 3.78 m/s, (e) Modified Ochi–Shin for 4.26 m/s and (f) Modified Ochi-Shin for 5.03 m/s.

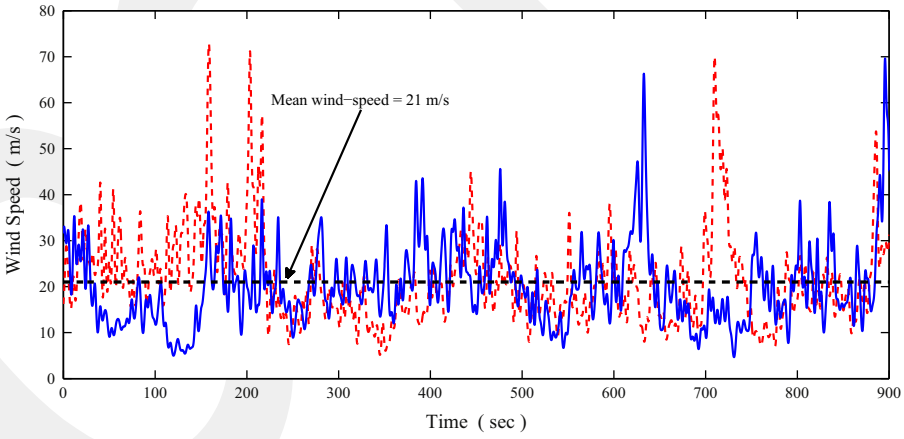

Fig. 4. Time-history for two of the generated 1000 samples of a random wind time history. The dashed horizontal line represents the target mean wind-speed of 21 m/s.

3. Results and discussion

Failure/fragility curves for Tree-1 and Tree-9 can be found in Figs. 6 and 7, respectively. The effect of decay on MCL is consistent for both trees in summer and winter: for a given wind speed, probability of failure increases as MCL increases. From Table 1, for example, for Tree-1 in summer, probability of failure for a maximum wind-speed of 70 mph is 12%, 21%, and 43% for a stem with no decay, 10% MCL and 20% MCL, respectively. For the same maximum wind speed for Tree-1 in winter, probability of failure is 1%, 2%, and 4% for a stem with no decay, 10% MCL and 20% MCL, respectively. For Tree-9 in summer, probability of failure for a maximum wind speed of 70 mph was similar to Tree-1: 10%, 18%, and 32% for a stem with no decay, 10% MCL and 20% MCL, respectively. For the same maximum wind speed for Tree-9 in winter, probability of failure is 22%, 37%, and 58% for a stem with no decay, 10% MCL and 20% MCL, respectively. It is important to note that the relationship between MCL and probability of failure is highly nonlinear with 20% MCL leading to increases in probability of failure of factors of 3–4.

To see the effect of season on probability of failure, the failure/fragility curves for Tree-1 and Tree-9 without decay are shown in Fig. 8. This figure shows that at a specific wind speed, the larger probability of failure occurred in different seasons for each tree. For Tree-1, probability of failure was larger in summer at a fixed wind speed, but the opposite was true for Tree-9. For example, the

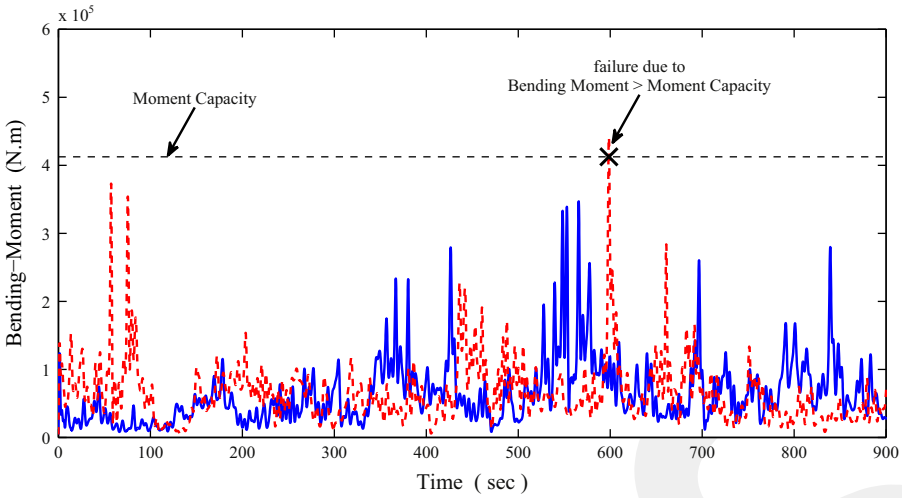

Fig. 5. Two independent samples of the random bending moment time history for Tree-1. The horizontal dashed line represents the yield moment of the undecayed tree and the ***X*** mark at approximately 600s shows an upcrossing of the yield moment corresponding to tree failure. The bending moments are computed at 1.4 m above ground level (breast height) and these samples correspond to wind time histories with a mean wind speed of 21 m/s.

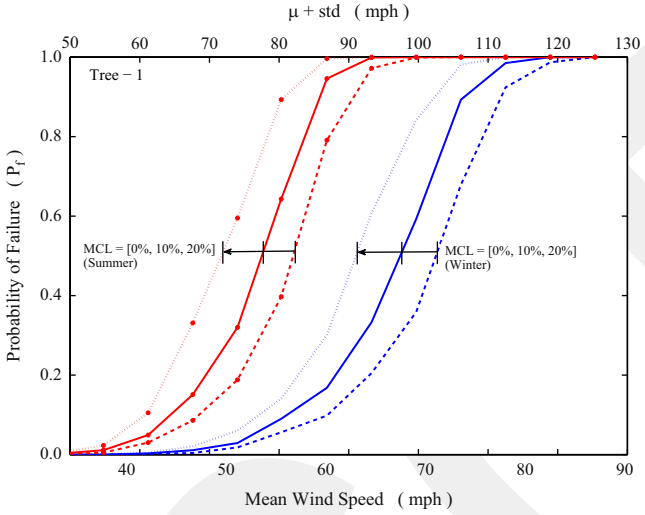

Fig. 6. Failure/fragility curves for Tree-1 in winter and summer with differing degrees of decay and resultant moment capacity loss. Curves with markers correspond to summer conditions and markerless curves correspond to winter conditions. Dual abscissas are used to indicate both the average wind speed during the analysis (lower axis) and a measure of the extreme wind speed (mean plus one standard deviation on the upper axis). Dotted, solid, and dashed lines represent, respectively, 0%, 10%, and 20% moment capacity loss (MCL) due to decay.

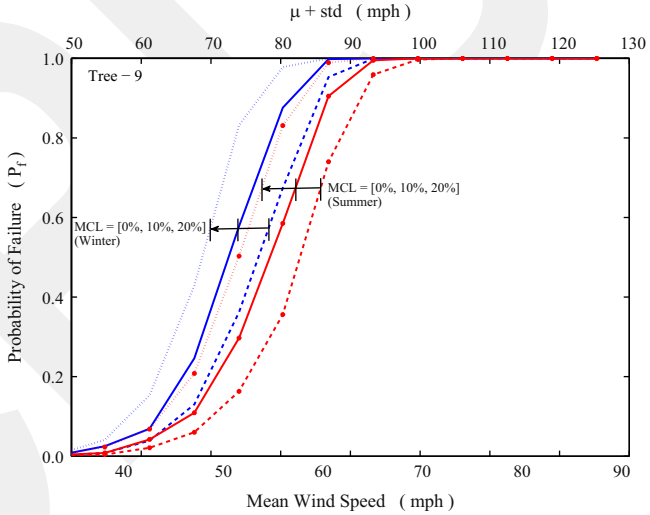

Fig. 7. Failure/fragility curves for Tree-9 in winter and summer with differing degrees of decay and resultant moment capacity loss. Curves with markers correspond to summer conditions and markerless curves correspond to winter conditions. Dual abscissas are used to indicate both the average wind speed during the analysis (lower axis) and a measure of the extreme wind speed (mean plus one standard deviation on the upper axis). Dashed, solid, and dotted lines represent, respectively, 0%, 10%, and 20% moment capacity loss (MCL) due to decay.

probability of failure of Tree-1 without decay at 55 mph was 40% and 5% in summer and winter, respectively. For the same conditions on Tree-9, however, the probability of failure was 36% and 67% in summer and winter, respectively. Since the moment capacity of the stem is assumed to be identical in winter and summer, changes in probability of failure must be due to changes in the bending moment in winter and summer. Specifically, Tree-9 must experience a larger moment at a given wind speed in winter than summer. The first order effect on bending moment is the frontal area, which is of course much larger in summer due to the presence of leaves. An important second order effect, however, is dynamic amplification, which is larger for Tree-9 in winter than summer, and, in the case of Tree-9, causes larger bending moment in winter.

To explain this finding further, consider the ratio

$$\frac{BM_S}{BM_W} = f\left[\frac{[(\rho AC_d),(\zeta)]_S}{[(\rho AC_d),(\zeta)]_W}\right] \tag{12}$$

Table 1
Comparison of the probability of exceedance values of Tree-1 and Tree-9 with respect to season and decay effects. All the values are taken from Figs. 6 and 7 when maximum wind-speed is 70 mph.

MCL	Summer (%)			Winter (%)		
	0	10	20	0	10	20
Tree-1	12	21	43	1	2	4
Tree-9	10	18	32	22	37	58

where BM is the wind-induced bending moment, and the subscripts S and W indicate the season (summer and winter, respectively). For a specific tree, the ratio of summer to winter wind-induced bending moments depends on the countervailing effects of changes in foliage on frontal area and dynamic amplification. The summer-to-winter changes in air density and drag coefficient are assumed to be the same for both trees and the moment

capacity is assumed to be independent of season. Therefore differences in the seasonal trend in the probability of failure must be attributed to the role of foliage in determining the bending moment in the stem of the tree. The loss of foliage as a season changes from summer to winter reduces the damping ratio and therefore increases the dynamic amplification factor. At the same time, the loss of foliage reduces the frontal area of the tree, leading to a reduction in loading. Therefore, whether a given tree will experience larger or smaller bending moments in winter as opposed to summer depends on the relative increase in bending moment due to reduced damping (increased dynamic amplification) and the reduction in loading due to reduced frontal area. It is expected that, for trees with very dense foliage, the loss in frontal area will dominate and therefore such trees will experience smaller bending moments and probabilities of failure in winter.

For the specific trees studied here, for Tree-1 the ratio of Eq. (12) is 1.53 indicating larger bending moments and probabilities of failure in summer. In contrast for Tree-9 the ratio of Eq. (12) is 0.87 indicating smaller bending moments and probabilities of failure in summer.

The effect of the ratio of damping ratios in summer and winter ζ_S/ζ_W on the dynamic response of each sugar maple in summer and winter can be estimated by (1) determining the ratio of frontal areas in summer and winter A_S/A_W, (2) parameterizing Eq. (12), the seasonal bending moment ratio, for each tree, and (3) setting Eq. (12) equal to the ratio of BM_S/BM_W as determined from the simulations for each tree. Figs. 9 and 10 show the best-fit lines describing BM_S/BM_W at six modeled wind speeds for Tree-1 and Tree-9, respectively. The mean slope of the six best-fit lines in Figs. 9 and 10 are 1.53 and 0.87 for Tree-1 and Tree-9, respectively. From the best-fit line in Fig. 2, for stem diameters of 53 cm and 66 cm, the predicted frontal areas in summer are 31 m^2 and 38 m^2 for Tree-1 and Tree-9, respectively. In winter, the estimated frontal areas of Tree-1 and Tree-9 are 8 m^2 and 15 m^2, respectively, indicating that Tree-9 retains more of its frontal area in winter. This means that Tree-9 experiences a smaller reduction in loading in winter. Thus, A_S/A_W is 3.9 and 2.5 for Tree-1 and Tree-9, respectively. Eqs. (13) and (14) illustrate the calculation of ζ_S/ζ_W for Tree-1; Eq. (15) and (16) illustrate the calculation for Tree-9.

$$\frac{BM_S}{BM_W}=f\left[\frac{[(\rho AC_d),(\zeta)]_S}{[(\rho AC_d),(\zeta)]_W}\right]_{Tree-1}=\frac{(1.226)(3.9A_W)(0.6)}{(1.326)(A_W)(1.0)}f\left[\frac{\zeta_S}{\zeta_W}\right]=1.53 \tag{13}$$

$$f\left[\frac{\zeta_S}{\zeta_W}\right]_{Tree-1}=0.71 \tag{14}$$

$$\frac{BM_S}{BM_W}=f\left[\frac{[(\rho AC_d),(\zeta)]_S}{[(\rho AC_d),(\zeta)]_W}\right]_{Tree-9}=\frac{(1.226)(2.5A_W)(0.6)}{(1.326)(A_W)(1.0)}f\left[\frac{\zeta_S}{\zeta_W}\right]=0.87 \tag{15}$$

$$f\left[\frac{\zeta_S}{\zeta_W}\right]_{Tree-9}=0.63 \tag{16}$$

Fig. 11 shows that the effect of damping ratio on dynamic amplification factor (R_d) varies with the excitation frequency of the wind. For excitation frequencies of 0.60 and 0.85 Hz, the ratio of R_d for summer (15%) and winter (5%) damping ratios (R_{d15}/R_{d5}) is 0.58 and 0.84, respectively. It can be seen that ζ_S/ζ_W for both trees (Eqs. (14) and (16)) is in the range of 0.58 and 0.84 The concept of dynamic amplification factor of Tree-1 was addressed in detail in [15].

In the treatment described here the change in natural frequency from summer to winter has not been considered. Published studies [45] and the authors measurements on open grown pear trees and forest grown red oaks have shown that the winter natural frequency is in the range of 1.5 to 2.0 times the summer

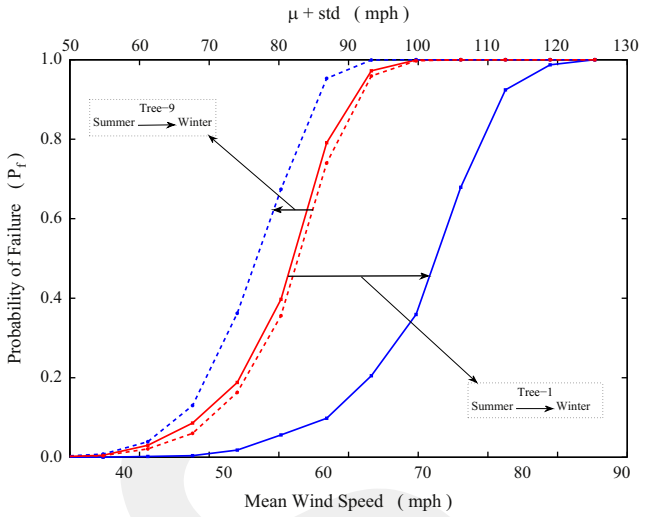

Fig. 8. Comparison of failure/fragility curves for undecayed (MCL=0%) states of Tree-1 and Tree-9 in the winter and summer seasons. Solid curves are for Tree-1 and dashed curves are for Tree-9. As in Figs. 6 and 7 dual horizontal axes are used to show the relationship of the probability of failure to the mean and mean plus one standard deviation wind speeds.

natural frequency. For the trees studied here, that change in frequency has an insignificant impact on the dynamic amplification. Thus, it may be assumed that the most important parameters are the external force effect and the damping ratio effect in order to obtain the failure/fragility curves for the winter season. With more extensive measurements or estimates of the leaf mass and winter natural frequency it would be possible to develop a model for the seasonal change in frequency.

It is difficult to compare previous studies of urban tree failure during wind events [6,46,47] to the current approach because of differences in the nature of the wind event and regional topography, as well as the fact that sugar maples have not been previously studied. In addition, studies of failed trees implicitly examine the rupture bending moment, while the current paper considered the yield bending moment. This would naturally induce failure at wind speeds of smaller magnitudes. Nevertheless, some qualitative comparisons are possible. In Charlotte, NC, USA, approximately 58% of 54 oaks that had a range of 5–20% loss in second moment of area due to decay failed during hurricane Hugo, which reached peak wind speeds at the study location of 90 mph [46]. The mean stem diameter of oaks was 57 cm [46]. Fig. 6 shows that the probability of failure for Tree-1 with leaves is about 98% and 100% for 10% MCL and 20% MCL, respectively. The disparity between the MC simulations and the findings for Hurricane Hugo [46] was likely due to several factors. The peak wind speed of 90 mph may not be representative of a 15 min episode with sustained mean wind speed at that level, nor is it clear how peak wind speed was measured in [46]. Differences between species with respect to crown architecture and wood properties [20] would alter frontal area [30], drag coefficient [30], damping ratio [17], and moment capacity. Previous studies have emphasized the importance of species as it relates to predicting failure [46,48–51]. Also during Hurricane Hugo, in Puerto Rico, the mean probability of failure for a range of tropical tree species was 0% and 80% for maximum wind speeds of 35 mph and 78 mph, respectively [46]. While Fig. 6 (Tree-1) shows that the probability of failure is 0 and 8% for 35 mph and 78 mph wind-speeds, respectively, Fig. 7 (Tree-9) shows that the probability of failure is 0% and 65% for the same wind speeds. Again, it is important to consider that the data of [46] include various species of varying stem diameters growing in different sites. According to [6], 2 species in the genus, *Pinus*, have

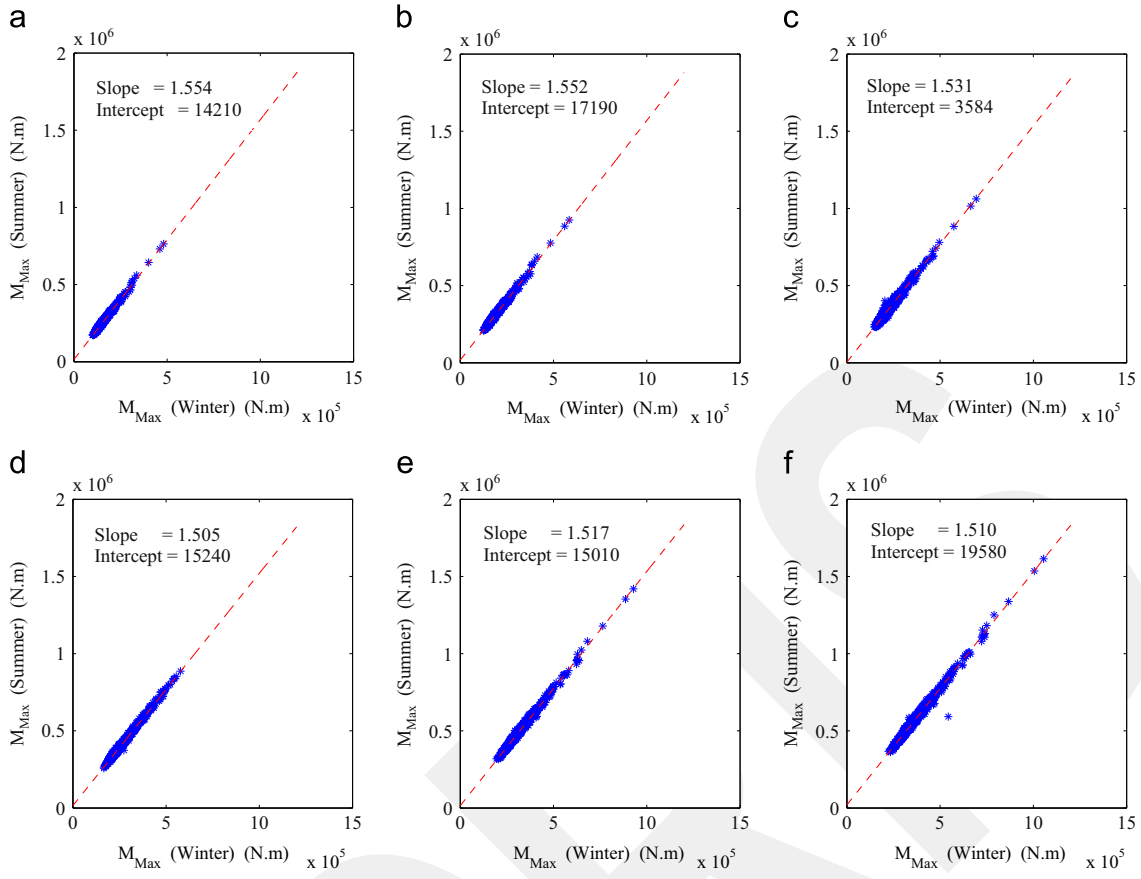

Fig. 9. The relationship between the maximum bending moments experienced in the stem of Tree-1 at 1.4 m above ground in summer and winter for varying mean wind-speed such as (19, 21, 23, 25, 27, and 29 m/s). (a) 19 m/s mean wind-speed, (b) 21 m/s mean wind-speed, (c) 23 m/s mean wind-speed, (d) 25 m/s mean wind-speed, (e) 27 m/s mean wind-speed and (f) 29 m/s mean wind-speed.

approximately 7% probability of failure at a mean wind speed of 67 mph. Figs. 6 and 7 show that the probability of failure is 20% and 100% for Tree-1 and Tree-9, respectively. One reason for this disparity may be that the trees considered in [6] were growing in a forested campground and therefore would have smaller frontal areas and less exposure to the wind. In forest stands, collisions with surrounding trees enhance damping [52]. It should also be noted that the probability of stem failure (in [49]) may be smaller than the results shown here due to poorly attached branches which would fail prior to the stem and therefore result in load shedding from the stem as the frontal area could be dramatically reduced.

Future studies should explore the probability of tree failure in a specific location for a given time period by using [14,53]

$$P_f^T = \int_0^\infty F_R(v) f_V(v) dv \tag{17}$$

where $F_R(v)$ is the failure/fragility curve function (as in Figs. 6 and 7) of trees in terms of wind speed (v), and $f_v(v)$ is the probability density function (pdf) of wind speed. For this probability of failure analysis, this wind-speed distribution can belong to location and can be expressed with reference to any time period (such as annual wind speed, 10-year wind speed, and 50-year wind speed).

4. Conclusion

A Monte Carlo based method for assessing the failure probability of trees subject to wind storms is presented in this paper. The key elements are a detailed finite element model of the tree, generation of stochastic wind time histories, dynamic time history analysis of the tree response to wind, and evaluation of failure probabilities at a range of mean wind speeds to generate failure/fragility curves. The method has been applied to two trees, and it has been shown how the method can be extended to account for decay and foliage. The trees themselves have been considered deterministic in material properties and geometry, and the probability of failure is therefore driven by randomness in the wind field.

The example trees differ in that Tree-1 has larger failure probability for summer than winter, but Tree-9 has smaller failure probability for summer than winter. This difference is caused by the subtle ways in which foliage affects frontal area, drag coefficient, and damping ratio. It appears that the total amount of foliage plays a key role in determining whether the probability of failure is larger in summer or winter. The two examples presented here show that season can affect probability of failure by as much as 40%. Moment capacity loss is shown to significantly affect probability of failure.

The results discussed in this paper should be considered in the context of the modeling assumptions used. One of the assumptions is that the Ochi–Shin spectrum was modified and calibrated by using small mean wind-speeds (from 1.1 m/s to 5.7 m/s), and then wind samples were generated by using this modified Ochi–Shin equation for larger mean wind-speeds (from 13 m/s to 39 m/s). The second assumption is that the effect of decay on tree dynamics such as natural frequency cannot be explicitly considered using the method presented here. The advantage of this method is that the Monte Carlo simulations need not be run repeatedly for every moment capacity loss value of interest. The third key assumption is that the relationship between stem diameter and frontal area is governed by Fig. 2, which was

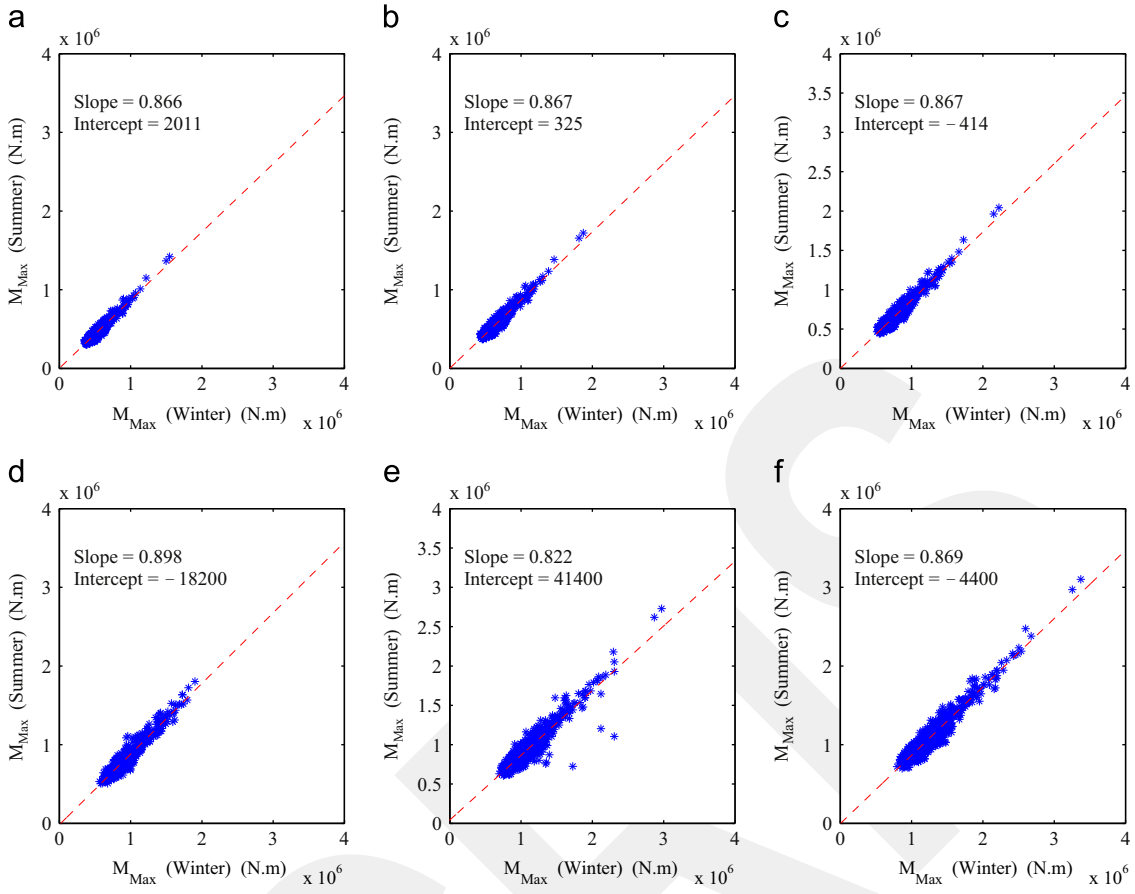

Fig. 10. The relationship between the maximum bending moments experienced in the stem of Tree-9 at 1.4 m above ground in summer and winter for varying mean wind-speed such as (19, 21, 23, 25, 27, and 29 m/s). (a) 19 m/s mean wind-speed, (b) 21 m/s mean wind-speed, (c) 23 m/s mean wind-speed, (d) 25 m/s mean wind-speed, (e) 27 m/s mean wind-speed and (f) 29 m/s mean wind-speed.

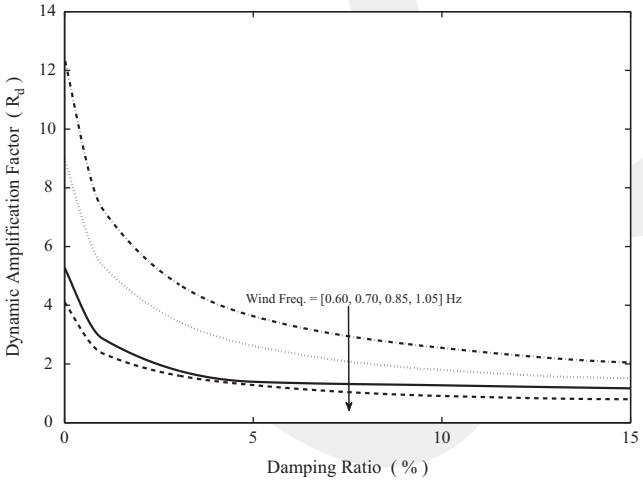

Fig. 11. Dynamic amplification factors for Tree-1 for a range of damping ratios and wind frequencies. The dependence of the dynamic amplification on damping ratio is an important factor in determining whether the summer state (15%, highly damped) or the winter state (5% modestly damped) generates the more critical bending moment and larger failure probabilities. The dashed, solid, dotted, and dashed and dotted curves are for the wind frequencies of 0.60, 0.70, 0.85, and 1.05 Hz, respectively.

measured on small trees of a different species. The final important assumption is that compressive yield stress and other parameters (such as damping ratios, drag coefficients, MOE, and MOR) used in the study are taken from the literature rather than measurements performed on the example trees.

In summary, the application of modeling of the probability of failure to individual open-grown trees through probabilistic, dynamic time history analysis is a novel contribution to risk assessment of amenity trees. The approach shown here is robust and is widely used in other engineering communities such as seismic design and evaluation [54–56] and with additional effort devoted to the modeling of tree mechanics this approach could become a useful and practical tool for risk assessment for individual amenity trees.

Acknowledgements

This study was funded by the TREE Fund's Mark S. McClure Biomechanics Fellowship.

References

[1] Nowak DJ, Dwyer JF. Understanding the benefits and costs of urban forest ecosystems. In: Kuser JE, editor. Handbook of urban and community forestry in the northeast. New York City, NY: Plenum Publishers; 2000. p. 11–25.
[2] Schmidlin T. Human fatalities from wind-related tree failures in the United States, 1995–2007. Nat Hazards 2009;50:13–25.
[3] Mortimer MJ, Kane B. Hazard tree liability in the United States: uncertain risks for owners and professionals. Urban For Urban Green 2004;2:159–165.
[4] Smiley ET, Matheny N, Lilly S. Tree risk assessment: a foundation. Arborist News 2011;20:12–20.
[5] Gardiner BA, Quine CP. Management of forests to reduce the risk of abiotic damage – a review with particular reference to the effects of strong winds. For Ecol Manag 2000;135:261–277.
[6] Kane B. Tree failure following a windstorm in Brewster, Massachusetts, USA. Urban For Urban Green 2008;7:15–23.

[7] Gardiner B, Byrne K, Hale S, Kamimura K, Mitchell SJ, Peltola H, et al. A review of mechanistic modelling of wind damage risk to forests. Anglais 2008;81:447–463.
[8] Miller KF. Windthrow hazard classification, H.M. Stationery Office; 1985.
[9] Mitchell SJ. A diagnostic framework for windthrow risk estimation. For Chron 1998;74:100–105.
[10] Peltola H, Kellomäki S, Väisänen H, Ikonen VP. A mechanistic model for assessing the risk of wind and snow damage to single trees and stands of Scots pine, Norway spruce, and birch. Can J For Res 1999;29:647–661.
[11] Blennow K, Andersson M, Sallnäs O, Olofsson E. Climate change and the probability of wind damage in two Swedish forests. For Ecol Manag 2010;259:818–830.
[12] Ancelin P, Courbaud B, Fourcaud T. Development of an individual tree-based mechanical model to predict wind damage within forest stands. For Ecol Manag 2004;203:101–121.
[13] Arwade SR, Deodatis G. Variability response functions for effective material properties. Probab Eng Mech 2011;26:174–181.
[14] Smith MA. A Monte Carlo based method for the dynamic performance analysis of tall buildings under turbulent wind loading. In: Civil Engineering, Northeastern University; 2009.
[15] Ciftci C, Brena SF, Kane B, Arwade SR. The effect of crown architecture on dynamic amplification factor of an open-grown sugar maple (*Acer saccharum* L.). Trees 2013;27:1175–1189.
[16] Kane B, Modarres-Sadeghi Y, James K, Reiland M. Effects of crown structure on the sway characteristics of large decurrent trees. Trees 2014;28:151–159.
[17] Kane B, James KR. Dynamic properties of open-grown deciduous trees. Can J For Res 2011;41:321–330.
[18] Reiland M. The effect of leaves and steel support cables on the dynamic properties of Northern Red Oak (Quercus rubra) with co-dominant trunks. Berlin Heidelberg: Springer; 2013 (Department of Environmental Conservation).
[19] Dahle GA, Grabosky JC. Variation in modulus of elasticity (E) along *Acer platanoides* L. (Aceraceae) branches. Urban For; Urban Green 2010;9:227–233.
[20] Kretschmann DE. Mechanical properties of wood. Wood handbook, wood as an engineering material. Madison, WI, U.S.: Department of Agriculture Forest Service, Forest Products Laboratory; 2010; 1–46.
[21] de Langre E. Effects of wind on plants. Annu Rev Fluid Mech 2008;40:141–168.
[22] Sellier D, Fourcaud T. Crown structure and wood properties: influence on tree sway and response to high winds. Am J Bot 2009;96:885–896.
[23] Hsu SA, Meindl EA, Gilhousen DB. Determining the power-law wind-profile exponent under near-neutral stability conditions at sea. J Appl Meteorol 1994;33:757–765.
[24] Zhu J, Matsuzaki T, Sakioka K. Wind speeds within a single crown of Japanese black pine (*Pinus thunbergii* Parl.). For Ecol Manag 2000;135:19–31.
[25] Panofsky HA, Dutton JA. Atmospheric turbulence: models and methods for engineering applications. New York: John Wiley & Sons; 1984.
[26] Kane B, Smiley ET. Drag coefficients and crown area estimation of red maple. Can J For Res 2006;36:1951–1958.
[27] Nowak DJ. Estimating leaf area and leaf biomass of open-grown deciduous urban trees. For Sci 1996;42:504–507.
[28] Peper PJ, McPherson EG, Mori SM. Predictive equations for dimensions and leaf area of coastal southern California street trees. J Arboric 2001;27:169–180.
[29] Peper PJ, McPherson EG, Mori SM. Equations for predicting diameter, height, crown width, and leaf area of San Joaquin Valley street trees. J Arboric 2001;27:306–317.
[30] Kane B, Pavlis M, Harris JR, Seiler JR. Crown reconfiguration and trunk stress in deciduous trees. Can J For Res 2008;38:1275–1289.
[31] Ochi MK, Shin VS. Wind turbulent spectra for design consideration of offshore structures, in: Proceedings of offshore technology conference; 1988.
[32] Shaw RH, Silversides RH, Thurtell GW. Some observations of turbulence and turbulent transport within and above plant canopies. Bound-Layer Meteorol 1974;5:429–449.
[33] Raupach MR, Shaw RH. Averaging procedures for flow within vegetation canopies. Bound-Layer Meteorol 1982;22:79–90.
[34] Wilson JD, Ward DP, Thurtell GW, Kidd GE. Statistics of atmospheric turbulence within and above a corn canopy. Bound-Layer Meteorol 1982;24:495–519.
[35] Baldocchi DD, Meyers TP. A spectral and lag-correlation analysis of turbulence in a deciduous forest canopy. Bound-Layer Meteorol 1988;45:31–58.
[36] Amiro BD. Drag coefficients and turbulence spectra within three boreal forest canopies. Bound-Layer Meteorol 1990;52:227–246.
[37] Gardiner BA. Wind and wind forces in a plantation spruce forest. Bound-Layer Meteorol 1994;67:161–186.
[38] Finnigan J. Turbulence in plant canopies. Annu Rev Fluid Mech 2000;32:519–571.
[39] Shinozuka M, Deodatis G. Simulation of stochastic processes by spectral representation. Appl Mech Rev 1991;44:191–204.
[40] Nataf A. D´etermination des distributions de probabilit´es dont les marges sont donn´ees. Comptes Rendus Acad Sci 1962:42–43.
[41] Garcia A, Torres JL, Prieto E, de Francisco A. Fitting wind speed distributions: a case study. Sol Energy 1998;62:139–144.
[42] Luna RE, Church HW. Estimation of long-term concentrations using a universal wind speed distribution. J Appl Meteorol 1974;10:910–916.
[43] Morgan EC, Lackner M, Vogel RM, Baise LG. Probability distributions for offshore wind speeds. Energy Convers Manag 2011;52:15–26.
[44] Ciftci C, Kane B, Brena SF, Arwade SR. Loss in moment capacity of tree stems induced by decay. Trees 2014;28:517–529.
[45] Baker CJ. Measurements of the natural frequencies of trees. J Exp Bot 1997;48:1125–1132.
[46] Francis JK, Gillespie AJR. Relating gust speed to tree damage in Hurricane Hugo. J Arboric 1989;19(1993):369–373.
[47] Smiley ET, Fraedrich BR. Relationship between tree morphology and growth stress in mature European beech stands. J Arboric 1992;18:201–204.
[48] Duryea ML, Kampf E, Ramon CL. Hurricanes and the urban forest II: effects on tropical and subtropical tree species. Arboric Urban For 2007;33:98–112.
[49] Gibbs JN, Greig BJW. Survey of parkland trees after the great storm of 16 October 1987. Arboric J 1990;14:321–347.
[50] Jim CY, Liu HHT. Storm damage on urban trees in Guangzhou, China. Landsc Urban Plan 1997;38:45–60.
[51] Putz FE, Sharitz RR. Hurricane damage to old growth forest in Congaree Swamp National Monument, South Carolina, USA, USDA forest service general technical report SR3-5; 1996, p. 92–100.
[52] Moore JR, Maguire DA. Natural sway frequencies and damping ratios of trees: influence of crown structure. Trees – Struct Funct 2005;19:363–373.
[53] Yue LI, Ellingwood BR. Hurricane damage to residential construction in the US: importance of uncertainty modeling in risk assessment. Eng Struct 2006;28:1009–1018.
[54] Ellingwood BR. Earthquake risk assessment of building structures. Reliab Eng Syst Saf 2001;74:251–262.
[55] Ramamoorthy SK. Seismic fragility estimates for reinforced concrete framed buildings. Department of Civil Engineering, College Station, TX, USA: Texas A&M University; 2006.
[56] Singhal A, Kiremidjian A. Method for probabilistic evaluation of seismic structural damage. J Struct Eng 1996;122:1459–1467.